Molecular Catalysis 577 (2025) 114991

Contents lists available at ScienceDirect

Molecular Catalysis

journal homepage: www.journals.elsevier.com/molecular-catalysis

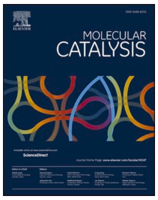

Research Paper

Theoretical insights of nitrate reduction to ammonia on partially reduced In_2O_3 surfaces

Qingchao Fang [a], Md Tarikal Nasir [a], Dimuthu Wijethunge [b], Yun Han [c], Xuxin Kang [d], Cheng Yan [e], Anthony P. O' Mullane [a], Hanqing Yin [a,f,*], Aijun Du [a,f]

[a] School of Chemistry and Physics, Queensland University of Technology (QUT), Gardens Point Campus, Brisbane, 4001, Australia
[b] School of Engineering, University of Southern Queensland, 37 Sinnathamby Blvd, Springfield Central QLD 4300, Australia
[c] School of Engineering and Built Environment, Queensland Micro- and Nanotechnology Centre, Griffith University, Nathan Campus, Nathan, Queensland 4111, Australia
[d] School of Physical Science and Technology, Ningbo University, Ningbo, PR China
[e] School of Mechanical, Medical and Process Engineering, Queensland University of Technology (QUT), Brisbane, QLD 4001, Australia
[f] QUT Centre for Materials Science, Queensland University of Technology, Gardens Point Campus, Brisbane, 4001, Australia

ARTICLE INFO

Keywords:
Nitrate reduction
Density functional theory
Indium oxide
Oxygen vacancy

ABSTRACT

The electrocatalytic nitrate reduction reaction (NO_3RR) has attracted much attention due to the formation of value-added ammonia as well as being an environmentally benign process. However, there is still a lack of high-performance electrocatalysts and an in-depth understanding of the electrocatalytic reaction mechanism for NO_3RR. Based on first-principles calculations, the partially reduced In_2O_{3-x} catalysts with different monolayers (MLs) of oxygen vacancies were examined for the electrochemical conversion of nitrate to ammonia. The thermodynamically favourable pathways were identified for the screened candidates with various MLs of oxygen vacancies from 0 to 3, and the Gibbs free energy evolution of the 2 MLs of oxygen vacancies was downhill. The catalysts' performance is highly associated with the oxygen vacancy layers, and In_2O_3 with 2 ML of oxygen vacancies exhibits the highest NO_3RR activity. The introduction of oxygen vacancies can enhance the interfacial charge density around In active sites. The PDOS comparison between 0 ML and 2 MLs unravelled that the oxygen vacancies can downshift the overall orbitals and make the defective In_2O_3 metallic, thus promoting the electron transfer for improved performance of NO_3RR. Meanwhile, the competing hydrogen evolution reaction (HER) is effectively inhibited. This work not only proposes a high-performance electrocatalyst for ammonia production but also reveals the relationship between the layer number of oxygen vacancies and the NO_3RR activity, thus highlighting vacancy engineering and providing novel insights into the design of NO_3RR catalysts.

1. Introduction

Ammonia (NH_3) is identified as a promising green hydrogen-rich fuel and is widely used in the production of nitrogen-containing fertilizers and chemicals such as pharmaceuticals, plastics and textiles [1,2]. The production of ammonia is considered one of the greatest inventions of the 20th century, which is centred around the energy-intensive Haber-Bosch process [3]. The process takes up around 1 % of the world's energy supply due to the demanding requirement of temperature (500 °C) and pressure (>200 atm), leading to 1.4 % of global CO_2 emissions annually [4]. To reduce the energy consumption and environmental impacts, alternative strategies, such as physical and chemical and biological treatments, are being explored for ammonia production [5]. However, many processes are time-consuming and require multiple steps under harsh conditions (specific pH, high pressure and H_2 feeding). In contrast, electrocatalysis is a promising option because of its ambient reaction conditions, renewable energy supply and environmental friendliness [6]. Previously, N_2 was regarded as the most promising nitrogen sources due to its abundance in the atmosphere. Although many attempts have been made to electrochemically produce ammonia from N_2, the production process is still plagued by issues such as large overpotential and the competing HER. For non-polar N_2 molecule, the strong $N\equiv N$ bond possesses a high bond energy of 941 kJ mol^{-1}, which makes it difficult to be captured and activated [7]. Therefore, there is an urgent need to search for new nitrogen sources for ammonia production.

Nitrate (NO_3^-) is a common pollutant of water resources and it may

---

* Corresponding author.
E-mail address: hanqing.yin@connect.qut.edu.au (H. Yin).

https://doi.org/10.1016/j.mcat.2025.114991
Received 16 December 2024; Received in revised form 26 February 2025; Accepted 2 March 2025

arise from fuel combustion, industrial sewage discharge and farming [8]. This high-valence-state nitrate, existing in the soil and underground water, is a toxic chemical which can harm biodiversity and human health [9,10]. Besides, the partial conversion of NO_3^- to NO_2^- can increase the risk of getting cancer and birth defects (blue baby syndrome and methemoglobinemia) [11,12]. Nevertheless, the low bond energy of the polar $N = O$ bond (204 KJ mol^{-1}), high solubility and abundance in wastewater make it a promising nitrogen source with more efficient ammonia production compared to N_2, while concomitantly allowing for reducing the impact of nitrate on the environment. The nitrate reduction reaction (NO_3RR) is complicated with potential formation of multiple intermediates via different pathways, which is associated with the transfer of eight electrons and nine protons as shown below:

$$NO_3^-(aq) + 9H^+(aq) + 8e^- \rightarrow NH_3(g) + 3H_2O\ (l) \tag{1}$$

The complete NO_3RR process is therefore environmentally friendly without harmful by-product formation. However, the intermediates may vary due to complex elementary steps, leading to varied overpotentials and final products. Moreover, the HER side reaction could inhibit ammonia production since the adsorbed H can block reactive sites, reduce the Faradaic Efficiency (FE) as well as contaminate the catalysts. Herein, it is reasonable to investigate the possible reaction pathways with preferred intermediates as well as evaluate the selectivity of the catalysts for efficient ammonia production.

To explore high-performance electrocatalysts, much attention has been devoted to TM-based candidates due to their unique electronic structure and earth abundance. Among noble TM-based electrocatalysts, Ru seems to be the most promising one for converting N-containing compounds to ammonia with high activity and selectivity [13]. By virtue of D-band centre modulation, Ru-doped materials are regarded as one of the most effective catalysts [14–16]. Besides Ru, Pd has been shown to be highly active, whose (111) facet exhibited a high FE of 79.91 % [17]. Nanostructured Ag and Ir were also synthesized and demonstrated high FEs of 96.4 % and 84.7 %, respectively [18,19]. Despite their potential for nitrate reduction, the use of noble metals is still hampered by high cost and scarcity. Therefore, nonprecious metals have been the centre of focus for the nitrate reduction reaction. Cu was widely investigated in terms of facet preference, oxidation state, defect engineering and synergy effect with other transition metals [20–23]. Through surface engineering, enhanced charge transfer or higher electronic density around the active site can promote the nitrate reduction process [21,24]. Besides, different types of substrates (nickel foam, MOF and Cu-PTCDA) can promote the hydrogenation of intermediates through the coordination regulation of Cu atoms [23,25,26]. Iron and iron-based alloys were also proven effective in catalysing the nitrate reduction reaction [27–29]. A high FE of 98 % for NO_3RR was also achieved on the 2D Fe-MoS_2 catalyst due to the influence of newly formed bonding/antibonding orbitals on stabilizing the NO intermediate [30]. Additionally, the performance of other TM-based electrocatalysts, such as Co, Ni and Ti, was also evaluated [31–33].

Recently, p-block elements, such as boron, indium and phosphorus, have aroused enthusiasm due to their promoting effect when doped into transition metal-based catalysts [34–38]. Liu *et al.* doped boron atoms in Cu electrodes through a one-step electrodeposition strategy, where a high FE of 92.74 % was achieved for the nitrate reduction to ammonia. The B doping led to the change in charge distribution and local coordination environment, which enhanced the nitrate adsorption and promoted the intermediate conversion [39]. Deng *et al.* have prepared Co_2B nanoparticles for nitrate reduction, where the Co-terminal surface exhibits a high NH_4^+ FE of 96.61 % [40]. The eco-friendly indium also plays an important role in the catalytic process of NO_x reactants. The In was deposited on Pd nanoparticles for nitrate reduction under ambient conditions, where the sub-monolayer In can act as binding sites for nitrate with lowered activation barriers [41]. An optimal In coverage of 40 % was obtained with the volcano-shape relationship between activity and In surface coverage. The single-atom alloy In-Pd bimetallene was synthesised, where the isolated single-atom Pd, surrounded by In, can boost the NO_3RR process with a NH_3 FE of 87.2 % [42]. The p-d hybridisation of In and Pd around the Fermi level enhanced the nitrate adsorption and reduced the energy barrier of the potential-determining step (PDS). Wang *et al.* have examined the catalytic potential of In-Cu single-atom alloy (In_1Cu) for NO_2^- reduction, where the dinuclear sites can enhance the adsorption of nitrite and optimize the reaction energetics [43]. Herein, most of the research work on NO_x reduction focuses on the synergistic effects of p-block elements, while the major active sites are still TMs. Recently, the exceptional catalytic potential of the pure p-block compounds was also highlighted, some of which were predicted to exhibit extraordinary performance with electrochemical steps being energetically downhill [44,45]. Motivated by the promoting effects of indium atoms, the pure p-block In-based catalysts were chosen for the study of nitrate reduction to ammonia. As an n-type semiconductor, indium oxide (In_2O_3) has attracted much attention as a photocatalyst due to its chemical stability and suitable band structure. However, the electrocatalytic activity of pure In_2O_3 is far from satisfactory for widespread applications. Additionally, the stable phase of $In_2O_{3\text{-}x}$ with a high degree of surface reduction has been reported [46,47], where the metallic indium were also reported under certain conditions. However, the NO_3RR catalytic performance of In_2O_3 and its relationship with the oxygen vacancies are rarely reported and still under debate.

In this work, the catalytic performance of pure p-block catalyst In_2O_3 with varied oxygen vacancies was systematically clarified using DFT calculations, which demonstrates that In_2O_3 with 2 ML of oxygen vacancies exhibits the highest activity for nitrate reduction. The electronic structure analysis has been conducted to explore the relationship between the catalytic activities and varied MLs of oxygen vacancies. Besides, the proton adsorption energies were also obtained to evaluate the competing side reaction (HER), where the positive values indicate the high selectivity of the $In_2O_{3\text{-}x}$ catalyst towards NO_3RR. Finally, the In_2O_3 catalyst with an optimum of 2 ML oxygen vacancies is proposed to be an attractive candidate with superior NO_3RR performance, thus not only expanding the application range of p-block elements for ammonia production but also providing insights into the rational design of efficient catalysts through vacancy engineering.

2. Computational details

First-principles calculations based on density functional theory (DFT) were conducted using the Vienna ab initio simulation package (VASP) [48,49]. The electron and ion interaction were described by the projector augmented wave (PAW) method [50]. The exchange-correlation approximation was estimated by a Perdew–Burke–Ernzerhof (PBE) functional [51,52]. The plane wave basis with a cut off energy of 450 eV was used. The energy and force threshold were 1×10^{-5} eV and 0.01 eV $Å^{-1}$, respectively. The Brillouin zone was sampled by employing the Monkhorst−Pack k-point mesh for the total energy calculation. The bulk structure of In_2O_3 was obtained from the Materials Project database [53]. The (111) surface was constructed with a 3 × 3 × 1 supercell and five layers were built to mimic the reactive slab. The bottom two layers were fixed, and the top three layers were relaxed without any constraint throughout the calculations. To avoid the influence of adjacent images, the vacuum thickness was set to at least 16 Å. To implement the van der Waals correction, Grimme's DFT-D3 method was adopted [54]. The solvent effect was considered by the implicit solvent model with the electric constant set to be 80 [55]. The charge density difference was evaluated and so was Bader charge analysis [56,57]. The free energies of H^+ are corrected by previous reports [58,59]. The projected density of states (PDOS) was analysed through VASPKIT which is an efficient pre- and post-processing program [60].

3. Results and discussion

Since the pristine In_2O_3 possess limited catalytic performance [41, 61], the surface electronic regulation through vacancy engineering seems practical for the NO_3RR process. From the perspective of availability, the partially reduced surface of In_2O_3 has already been reported experimentally [47,62,63], and also quantified by theoretical works [64,65]. Among the studied facets, the $In_2O_3(111)$ surface is the most stable one which is already fabricated in the lab [66–68]. The structure of $In_2O_{3\text{-}x}$ with negative formation energies of oxygen vacancies is demonstrated in Fig. 1(a), where the top five monolayers of oxygen atoms were sequentially removed as previously reported [69]. The number of oxygen atom removal layers, ranging from 0 to 3, was chosen for study, where 0 layer acts as a reference and 3 layers expose the metallic In on the surface. The other 4 and 5 layers were excluded since the 3-layer model already exhibits high instability based on electrochemical stability analysis [70,71]. The adsorption of nitrate on the surface is the first step for nitrate reduction. Due to the complex surface atomic structure, the initial adsorption configurations of nitrate onto the slabs were checked on different sites (top, bridge and hollow sites, etc.) as well as nitrate ion orientations. The possible adsorption configurations and free energies were shown in Figure S1, where the most thermodynamically favourable ones were selected as shown in Fig. 1(b).

It should be noted that the nitrate adsorption on pure In_2O_3 without oxygen vacancy is thermodynamically unfavourable, which was thus excluded for the electrochemical reduction of nitrate to ammonia. In comparison, the nitrate adsorptions on the other defective surfaces were favoured. The adsorption energy increases with MLs and the adsorption configuration changes from the 3-O pattern to the 2-O pattern accordingly. Besides, the bond length of N—O also increased above 1.23 Å, indicating that the adsorbed nitrate is captured and activated for further reduction.

The reaction pathway is a complicated process which involves the deoxygenation and hydrogenation stages of various intermediates. Besides, the adsorption of key intermediates can lead to different reaction pathways as shown in Table S1. As shown in Fig. 2, the commonly reported reaction pathways for NO_3RR are demonstrated according to different adsorption configurations of NO. Initially, the adsorbed nitrate ions would be attacked by a proton-electron pair, leading to the formation of NO_2 with one water molecule released. Afterwards, NO_2 would also be reduced to NO. The direct deoxygenation of NO has been widely reported [72,73], which can be described as $NO_3^-(l) \rightarrow {}^*NO_3 \rightarrow {}^*NO_2 \rightarrow {}^*NO \rightarrow {}^*N \rightarrow {}^*NH \rightarrow {}^*NH_2 \rightarrow {}^*NH_3 \rightarrow NH_3(g)$. In addition, the formation of $N_xH_yO_z$, such as NHO, NOH and NH_2OH, was also observed experimentally during the NO_3RR process [74,75], which was predicted by theoretical calculations and the key intermediate *NOH/*NHO was thought to be critical to the catalysts' performance [76–78]. Thus, the O-end or NO-side pathway was also considered, which can be $NO_3^-(l) \rightarrow {}^*NO_3 \rightarrow {}^*NO_2 \rightarrow {}^*NO \rightarrow {}^*NOH/{}^*NHO \rightarrow {}^*NH_2O \rightarrow {}^*NH_2OH \rightarrow {}^*NH_2 \rightarrow {}^*NH_3 \rightarrow NH_3(g)$. Apart from the mentioned reaction pathways, other complicated ones can be obtained partially due to the change of intermediate configuration during the hydrogenation process. One such complicated pathway was confirmed in this work as indicated by the green arrows.

To explore the catalytic performance of In_2O_3 with various MLs of oxygen vacancies, the thermodynamically favourable reaction pathway, based on the Gibbs free energy change (ΔG), is identified. The criterion for intermediate preference at every bifurcation point is the Gibbs free energy difference. The Gibbs free energy evolution of nitrate reduction on the three reduced slabs is displayed in Fig. 3. After the adsorption of nitrate ions on reduced In_2O_3 with 1 ML of oxygen vacancies, the generation of NO_2^- is a spontaneous process with a ΔG of -1.42 eV, followed by *NO formation in an exothermic manner. For the first two deoxygenation steps, byproduct formation is also evaluated, where the desorption of NO_2 and NO is found to be difficult with energy demands of 1.58 eV and 0.72 eV, respectively. The hydrogenation of the *NO intermediate may lead to the preferred formation of *NHO with a free energy change of -0.86 eV, as compared to the formation of *NOH with an increased ΔG of 0.27 eV. Similarly, the further hydrogenation of *NHO leads to the formation of $^*NH_2O$ instead of *NHOH with ΔG of -0.33 eV and 0.23 eV, respectively. For the conversion of $^*NH_2O$ to $^*NH_2OH$, an energy demand of 0.47 eV is required, which is also the PDS for the whole pathway. The desorption of possible byproduct NH_2OH is easy due to the free energy change of only 0.02 eV. After the conversion of $^*NH_2$ to $^*NH_3$ ($\Delta G = 0.13$ eV), the desorption of ammonia only requires 0.02 eV, indicating the easy desorption of the final product. A similar pathway can also be found for the In_2O_3 with 3 MLs of oxygen vacancies, while the PDS changes to the conversion of $^*NH_2OH$ to $^*NH_2$ with a limiting potential of 0.41 V. For the 2-ML case, the reduction of nitrate, in contrast, follows the NOH pathway, resulting in different intermediates (*NOH and *NHOH) with a downhill evolution of Gibbs free energy change. The final desorption of ammonia requires an energy demand of 0.12 eV. The high activity of In_2O_3 with 2 MLs of oxygen vacancies was also confirmed in consideration of solvation as shown in Figure S2. The solvation effect plays a minor role in the catalytic performance of the candidate. Among the three candidates, the reduced In_2O_3 with 2 ML of oxygen vacancies exhibits amazing NO_3RR activity with a limiting potential of 0 V. It can be concluded that the number of oxygen vacancies is closely related to the NO_3RR activity, and the different MLs of oxygen vacancies not only affect the nitrate adsorption but also lead to different intermediates and reaction pathways. The pH effect on three candidates was also evaluated in Fig. S3, where the catalytic performance of 2 ML model is still the highest among the three models. The corresponding PDS changes from $^*NH_2OH \rightarrow {}^*NH_2$ to $^*NO_2$

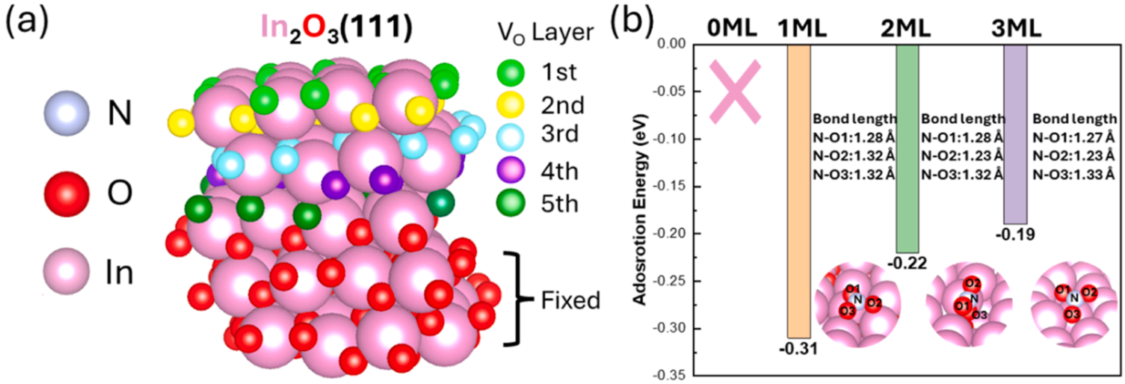

Fig. 1. (a) The configuration of $In_2O_{3\text{-}x}$ (111) surface with different layers of oxygen vacancies (V_O), while the bottom two layers were fixed to mimic the slab. (b) The thermodynamically favourable configurations of NO_3^- species adsorbed on the In_2O_3 catalysts with varied monolayers of oxygen vacancies.

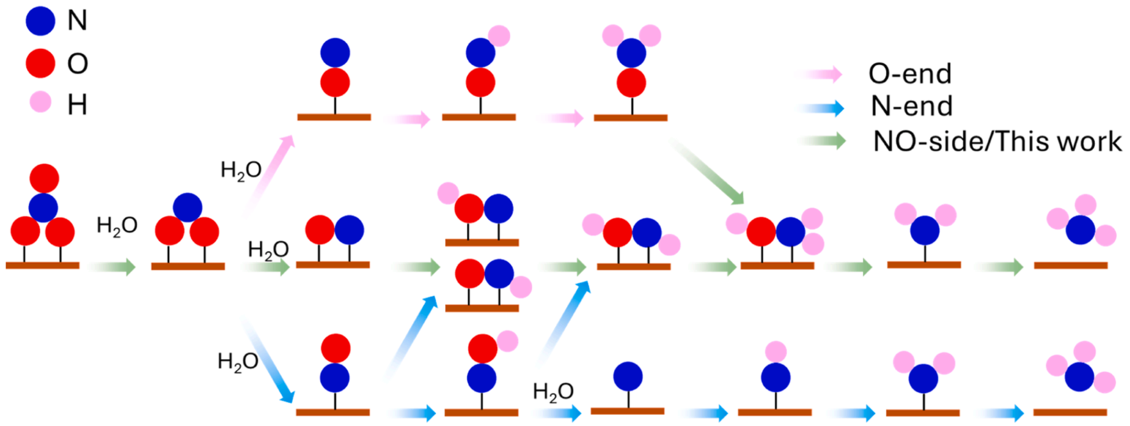

Fig. 2. Schematic illustration of three typical nitrate reduction pathways (O-end, N-end and NO-side) with this work involved. The pink, green and blue arrows are classified by different adsorption configurations of the *NO intermediate.

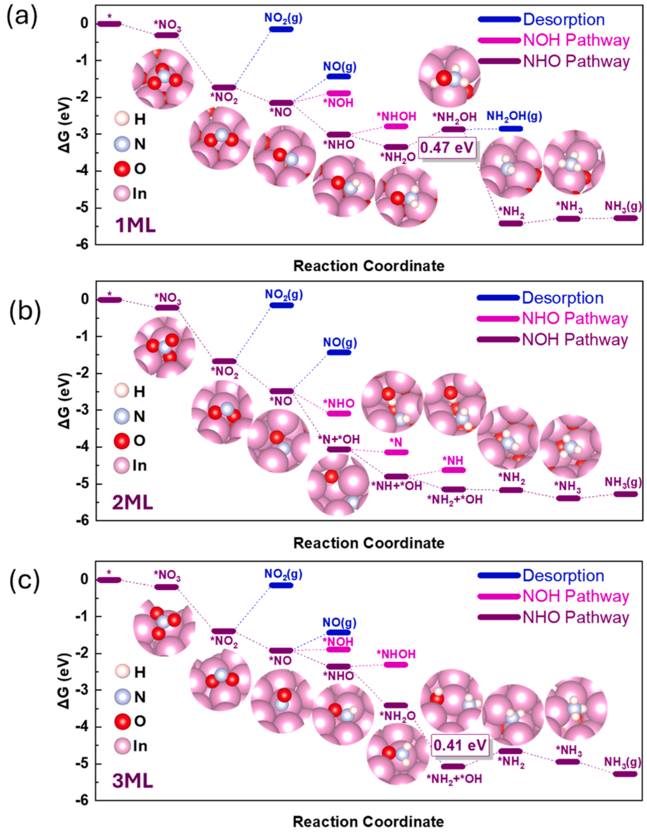

Fig. 3. The Gibbs free-energy diagram for NO_3RR on partially reduced $In_2O_3(111)$ surface with (a)1 ML, (b)2 MLs and (c)3 MLs of oxygen vacancies at 298.15 K, where the NOH and NHO pathways are also considered. The corresponding intermediates are included in the most thermodynamically favourable pathway (colour scheme: pink, In; red, O; white, H).

→ *NO, while the other two remain unchanged for different pH values.

To further elucidate the underlying mechanism for the NO_3RR process, the electronic density distribution, PDOS and charge density analysis were conducted. As shown in Fig. 4, the electron localization function (ELF) analysis for slabs with varied MLs was conducted and visualized. The higher ELF value (marked in red) indicates the higher electron localization, while a lower value (marked in blue) suggests there may be no electrons. With the introduction of various MLs of oxygen vacancies, notable electron redistribution was observed, and the increased charge density may contribute to the catalytic performance. Besides, the electronic structure comparisons between 0 ML and 2 ML were also conducted. An energy gap was observed between the valence band maximum (VBM) and conduction band minimum (CBM) for In_2O_3 with 0 ML of oxygen vacancies.

In contrast, the introduction of oxygen vacancies (2 ML) downshifted the overall orbitals and made the reduced In_2O_{3-x} metallic, which can reduce the energy barrier for electron transfer and aid in the process of NO_3RR. The charge transfer was visualized for nitrate adsorption on In_2O_3 with 2 ML of oxygen vacancies, where ample electrons (around 0.99 e^-) were transferred to the adsorbed nitrate.

The competitive HER was also evaluated due to the close thermodynamic potentials of the NO_3RR and HER [79]. For one thing, the proton may adsorb onto the surface and block the reactive sites for nitrate reduction. On the other hand, protons can form H_2 and desorb from the slab easily, reducing the FE significantly. As shown in Fig. 5, the adsorption sites and energy of the proton were thus plotted to assess the HER performance, and the free energy of proton adsorption (−0.09 eV) on Pt|C was included for comparison. It can be concluded that for all the In_2O_3 with 1 ML, 2 MLs and 3 MLs of oxygen vacancies, the adsorption of the proton on top, hollow and bridge sites is difficult since the values of the related adsorption energy are positive. Besides, other N—N coupling processes were also examined considering high NO_x coverage. As shown in Figure S4, the higher limiting potentials denote the preferred ammonia synthesis on the catalyst. Thus, the catalyst might be inactive towards byproduct formation, demonstrating excellent NO_3RR selectivity on reduced In_2O_3 surfaces.

4. Conclusions

In summary, the electrocatalytic performance of partially reduced In_2O_3 catalysts for the NO_3RR process was investigated based on the first-principles calculations. The catalyst with an optimum of 2 MLs of oxygen vacancies exhibited the highest activity with a thermodynamically downhill pathway identified through the free energy comparison of intermediates. ELF, PDOS and charge density analysis offer insights into the relationship between oxygen vacancies and catalytic activities. Furthermore, the excellent selectivity towards ammonia was demonstrated. By-product formation, such as NO_2, NO and NH_2OH, was evaluated, all of which are hard to desorb from the slab and the HER performance is very poor with adsorption free energies being very positive. Our theoretical work shows the relationship between the monolayer number of oxygen vacancies and NO_3RR activity, and the partially reduced In_2O_3 with 2 ML of oxygen vacancies can be an exceptional electrocatalyst for ammonia reduction, thus providing insights into the novel design of the NO_3RR electrocatalysts.

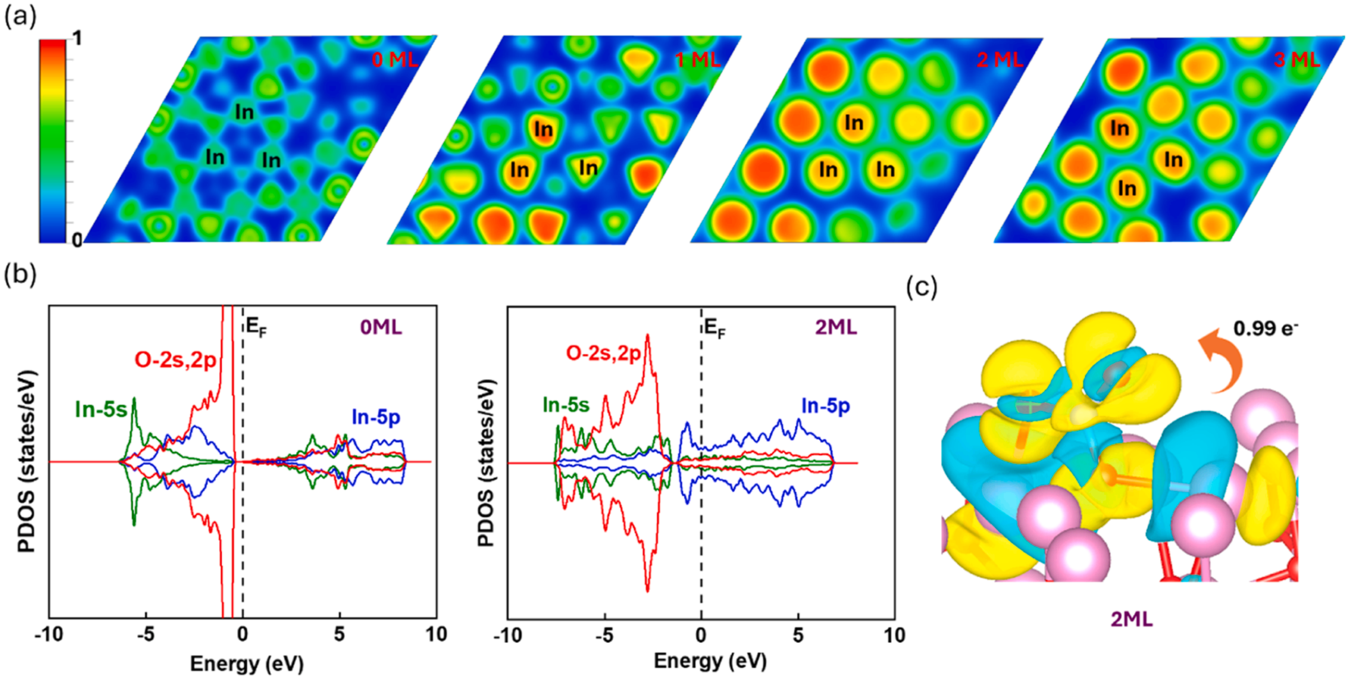

Fig. 4. (a) The electron localization function (ELF) contour for $In_2O_3(111)$ surface with varied MLs of oxygen vacancy. (b)PDOS for In_2O_3 with 0 ML and 2 ML oxygen vacancy. The Fermi level is aligned at zero. (c) The corresponding Bader charge transfer and charge density difference of nitrate ion adsorbed on the partially reduced $In_2O_3(111)$ surface. The value of the isosurface is set as 0.001 e/bohr^3. Yellow and blue regions represent the electron accumulation and depletion, respectively.

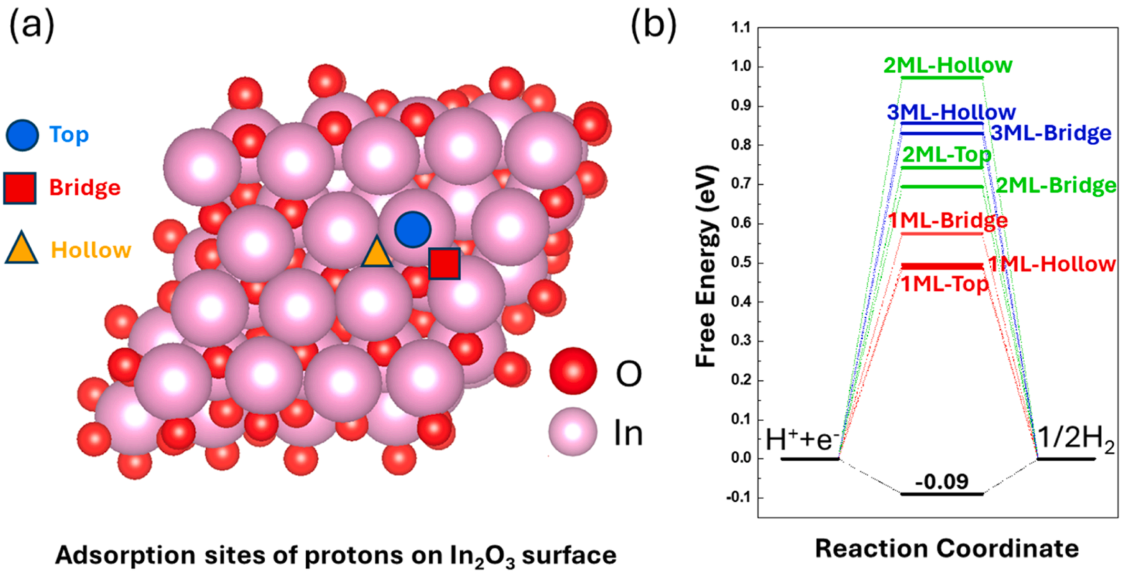

Fig. 5. (a) Top view of possible proton adsorption sites on the partially reduced $In_2O_3(111)$ surface, where the blue circle indicates the top of indium atoms, red rectangle as the bridge of indium atoms and yellow triangle as the hollow sites. (b) Free energy diagram of proton adsorption on different sites for reduced $In_2O_3(111)$ with 1 ML, 2 MLs and 3 MLs of oxygen vacancies, where the commercial Pt|C catalyst was also plotted as reference.

Data availability

The data supporting this article has been included as part of the Supplementary Information and is also available upon reasonable request.

CRediT authorship contribution statement

Qingchao Fang: Writing – original draft, Visualization, Validation, Methodology, Formal analysis, Data curation. **Md Tarikal Nasir:** Writing – review & editing, Validation, Formal analysis. **Dimuthu Wijethunge:** Writing – review & editing, Formal analysis. **Yun Han:** Writing – review & editing, Validation, Methodology, Formal analysis. **Xuxin Kang:** Writing – review & editing, Validation, Formal analysis. **Cheng Yan:** Writing – review & editing, Supervision, Methodology, Formal analysis. **Anthony P. O' Mullane:** Writing – review & editing, Supervision, Methodology, Formal analysis. **Hanqing Yin:** Writing – review & editing, Writing – original draft, Supervision, Investigation, Formal analysis, Conceptualization. **Aijun Du:** Writing – review & editing, Writing – original draft, Supervision, Resources, Project administration, Investigation, Funding acquisition, Formal analysis, Conceptualization.

Declaration of competing interest

The authors declare that they have no known competing financial interests or personal relationships that could have appeared to influence the work reported in this paper.

Acknowledgements

The authors acknowledge the high-performance computer resources granted by the NCI National Facility, and The Pawsey Supercomputing Centre via the National Computational Merit Allocation Scheme (NCMAS) supported by the Australian Government and the Government of Western Australia. A.D. greatly acknowledges funding support by the Australian Research Council of the Discovery Project (DP210100721).

Supplementary materials

Supplementary material associated with this article can be found, in the online version, at doi:10.1016/j.mcat.2025.114991.

References

[1] L. Fenn, L. Hossner, Ammonia volatilization from ammonium or ammonium-forming nitrogen fertilizers, Adv. Soil Sci. 1 (1985) 123–169.
[2] B. Pan, S.K. Lam, A. Mosier, Y. Luo, D. Chen, Ammonia volatilization from synthetic fertilizers and its mitigation strategies: a global synthesis, Agric. Ecosyst. Environ. 232 (2016) 283–289.
[3] A. Vojvodic, A.J. Medford, F. Studt, F. Abild-Pedersen, T.S. Khan, T. Bligaard, J. Nørskov, Exploring the limits: a low-pressure, low-temperature haber–bosch process, Chem. Phys. Lett. 598 (2014) 108–112.
[4] L. Wang, M. Xia, H. Wang, K. Huang, C. Qian, C.T. Maravelias, G.A. Ozin, Greening ammonia toward the solar ammonia refinery, Joule 2 (2018) 1055–1074.
[5] W.-J. Choi, J.-H. Kwak, S.-S. Lim, H.-J. Park, S.X. Chang, S.-M. Lee, M.A. Arshad, S.-I. Yun, H.-Y. Kim, Synthetic fertilizer and livestock manure differently affect δ^{15}n in the agricultural landscape: a review, Agric. Ecosyst. Environ. 237 (2017) 1–15.
[6] J. Masa, C. Andronescu, W. Schuhmann, Electrocatalysis as the nexus for sustainable renewable energy: the gordian knot of activity, stability, and selectivity, Angew. Chemie Int. Ed. 59 (2020) 15298–15312.
[7] D.S. Bem, C.P. Gibson, H.C. zur Loye, Synthesis of intermetallic nitrides by solid-state precursor reduction, Chem. Mater. 5 (1993) 397–399.
[8] B.T.S. Wu, C. Rivera, Y. Yuan, Nitrate and nitrite fertilizer production from air and water by continuous flow liquid-phase plasma discharge, J. Environ. Chem. Eng. 9 (2021) 104761.
[9] J. Camargo, J. Ward, Nitrate (no_3-n) toxicity to aquatic life: a proposal of safe concentrations for two species of nearctic freshwater invertebrates, Chemosphere 31 (1995) 3211–3216.
[10] G.A. Norris, Impact characterization in the tool for the reduction and assessment of chemical and other environmental impacts: methods for acidification, eutrophication, and ozone formation, J. Ind. Ecol. 6 (2002) 79–101.
[11] L. Knobeloch, B. Salna, A. Hogan, J. Postle, H. Anderson, Blue babies and nitrate-contaminated well water, Environ. Health Perspect. 108 (2000) 675–678.
[12] L. Lin, S. St Clair, G.D. Gamble, C.A. Crowther, L. Dixon, F.H. Bloomfield, J. E. Harding, Nitrate contamination in drinking water and adverse reproductive and birth outcomes: a systematic review and meta-analysis, Sci. Rep. 13 (2023) 563.
[13] H. Yin, A. Du, Revealing the potential of ternary medium-entropy alloys as exceptional electrocatalysts toward nitrogen reduction: an example of heusler alloys, ACS Appl. Mater Interfaces 14 (2022) 15235–15242.
[14] S. Bunea, K. Clemens, A. Urakawa, Electrified conversion of contaminated water to value: selective conversion of aqueous nitrate to ammonia in a polymer electrolyte membrane cell, ChemSusChem. 15 (2022) e202102180.
[15] J. Wu, Y.-X. Yu, Highly selective electroreduction of nitrate to ammonia on a ru-doped tetragonal co_2p monolayer with low-limiting overpotential, Catal. Sci. Technol. 11 (2021) 7160–7170.
[16] L. Lv, Y. Shen, J. Liu, X. Meng, X. Gao, M. Zhou, Y. Zhang, D. Gong, Y. Zheng, Z. Zhou, Computational screening of high activity and selectivity tm/g-c_3n_4 single-atom catalysts for electrocatalytic reduction of nitrates to ammonia, J. Phys. Chem. Lett. 12 (2021) 11143–11150.
[17] Y. Han, X. Zhang, W. Cai, H. Zhao, Y. Zhang, Y. Sun, Z. Hu, S. Li, J. Lai, L. Wang, Facet-controlled palladium nanocrystalline for enhanced nitrate reduction towards ammonia, J. Colloid Interface Sci. 600 (2021) 620–628.
[18] Z. Liu, C. Wang, C. Chen, C. Li, C. Guo, Selective electroreduction of nitrate to ammonia with high faradaic efficiency on nanocrystalline silver, Electrochem. Commun. 131 (2021) 107121.
[19] J.-Y. Zhu, Q. Xue, Y.-Y. Xue, Y. Ding, F.-M. Li, P. Jin, P. Chen, Y. Chen, Iridium nanotubes as bifunctional electrocatalysts for oxygen evolution and nitrate reduction reactions, ACS Appl. Mater Interfaces 12 (2020) 14064–14070.
[20] J. Qin, L. Chen, K. Wu, X. Wang, Q. Zhao, L. Li, B. Liu, Z. Ye, Electrochemical synthesis of ammonium from nitrates via surface engineering in cu_2o (100) facets, ACS. Appl. Energy Mater. 5 (2021) 71–76.
[21] Y. Wang, W. Zhou, R. Jia, Y. Yu, B. Zhang, Unveiling the activity origin of a copper-based electrocatalyst for selective nitrate reduction to ammonia, Angewandte Chemie Int. ed. 59 (2020) 5350–5354.
[22] J. Yuan, Z. Xing, Y. Tang, C. Liu, Tuning the oxidation state of cu electrodes for selective electrosynthesis of ammonia from nitrate, ACS Appl. Mater. Interfaces 13 (2021) 52469–52478.
[23] J. Li, J. Gao, T. Feng, H. Zhang, D. Liu, C. Zhang, S. Huang, C. Wang, F. Du, C. Li, Effect of supporting matrixes on performance of copper catalysts in electrochemical nitrate reduction to ammonia, J. Power Sources 511 (2021) 230463.
[24] X. Wang, M. Zhu, G. Zeng, X. Liu, C. Fang, C. Li, A three-dimensional cu nanobelt cathode for highly efficient electrocatalytic nitrate reduction, Nanoscale 12 (2020) 9385–9391.
[25] Z. Gao, Y. Lai, Y. Tao, L. Xiao, L. Zhang, F. Luo, Constructing well-defined and robust th-mof-supported single-site copper for production and storage of ammonia from electroreduction of nitrate, ACS. Cent. Sci. 7 (2021) 1066–1072.
[26] G.-F. Chen, Y. Yuan, H. Jiang, S.-Y. Ren, L.-X. Ding, L. Ma, T. Wu, J. Lu, H. Wang, Electrochemical reduction of nitrate to ammonia via direct eight-electron transfer using a copper–molecular solid catalyst, Nat. Energy 5 (2020) 605–613.
[27] W. Duan, G. Li, Z. Lei, T. Zhu, Y. Xue, C. Wei, C. Feng, Highly active and durable carbon electrocatalyst for nitrate reduction reaction, Water Res. 161 (2019) 126–135.
[28] Z.A. Jonoush, A. Rezaee, A. Ghaffarinejad, Electrocatalytic nitrate reduction using fe_0/fe_3o_4 nanoparticles immobilized on nickel foam: selectivity and energy consumption studies, J. Cleaner Prod. 242 (2020) 118569.
[29] Y. Wang, L. Zhang, Y. Niu, D. Fang, J. Wang, Q. Su, C. Wang, Boosting nh_3 production from nitrate electroreduction via electronic structure engineering of fe_3c nanoflakes, Green. Chem. 23 (2021) 7594–7608.
[30] J. Li, Y. Zhang, C. Liu, L. Zheng, E. Petit, K. Qi, Y. Zhang, H. Wu, W. Wang, A. Tiberj, 3.4% solar-to-ammonia efficiency from nitrate using fe single atomic catalyst supported on mos_2 nanosheets, Adv. Funct. Mater. 32 (2022) 2108316.
[31] N.C. Kani, J.A. Gauthier, A. Prajapati, J. Edgington, I. Bordawekar, W. Shields, M. Shields, L.C. Seitz, A.R. Singh, M.R. Singh, Solar-driven electrochemical synthesis of ammonia using nitrate with 11% solar-to-fuel efficiency at ambient conditions, Energy Environ. Sci. 14 (2021) 6349–6359.
[32] Q. Yao, J. Chen, S. Xiao, Y. Zhang, X. Zhou, Selective electrocatalytic reduction of nitrate to ammonia with nickel phosphide, ACS Appl. Mater Interfaces 13 (2021) 30458–30467.
[33] R. Jia, Y. Wang, C. Wang, Y. Ling, Y. Yu, B. Zhang, Boosting selective nitrate electroreduction to ammonium by constructing oxygen vacancies in tio_2, ACS. Catal. 10 (2020) 3533–3540.
[34] X. Yu, P. Han, Z. Wei, L. Huang, Z. Gu, S. Peng, J. Ma, G. Zheng, Boron-doped graphene for electrocatalytic n_2 reduction, Joule 2 (2018) 1610–1622.
[35] J. Crawford, H. Yin, A. Du, A.P. O'Mullane, Nitrate-to-ammonia conversion at an insn-enriched liquid-metal electrode, Angewandte Chemie Int. Ed. 61 (2022) e202201604.
[36] H. Yin, A. Du, Emerging role of p-block element in catalyzing electrochemical nox reduction to ammonia: a theoretical perspective, Adv. Funct. Mater., 2403718.
[37] H. Yin, A. Du, Boosting nitrogen reduction activity by defect engineering in 2d iron monochalcogenides fex (x= s, se), Small. Struct. 3 (2022) 2200107.
[38] J. Yuan, H. Yin, X. Jin, D. Zhao, Y. Liu, A. Du, X. Liu, A.P. O'Mullane, A practical fep nanoarrays electrocatalyst for efficient catalytic reduction of nitrite ions in wastewater to ammonia, Appl. Catal. B: Environ. 325 (2023) 122353.
[39] W. Liu, J. Chen, Y. Wei, Y. He, Y. Huang, M. Wei, Y. Yu, N. Yang, W. Zhang, L. Zhang, Regulating local electron distribution of cu electrocatalyst via boron doping for boosting rapid absorption and conversion of nitrate to ammonia, Adv. Funct. Mater. 34 (2024) 2408732.
[40] X. Deng, S. Xia, H. Zhao, J. Wang, Z. Wang, A. Kuklin, H. Ågren, G. Baryshnikov, H. Zhang, A new strategy for boron cluster-based metal boride (co_2b) synthesis and its applicability to electrocatalytic nitrate reduction, Chem. Eng. J. 485 (2024) 149639.
[41] S. Guo, K. Heck, S. Kasiraju, H. Qian, Z. Zhao, L.C. Grabow, J.T. Miller, M.S. Wong, Insights into nitrate reduction over indium-decorated palladium nanoparticle catalysts, ACS. Catal. 8 (2018) 503–515.
[42] M. Xie, S. Tang, Z. Li, M. Wang, Z. Jin, P. Li, X. Zhan, H. Zhou, G. Yu, Intermetallic single-atom alloy in–pd bimetallene for neutral electrosynthesis of ammonia from nitrate, J. Am. Chem. Soc. 145 (2023) 13957–13967.
[43] F. Wang, S. Shang, Z. Sun, X. Yang, K. Chu, Electrocatalytic nitrite reduction to ammonia on in_1cu single atom alloy, Chem. Eng. J. 489 (2024) 151410.
[44] H. Yin, X. Mao, S. Bell, D. Golberg, A. Du, Transition-metal-free, pure p-block alloy electrocatalysts for the highly efficient nitrate reduction to ammonia, Chem. Mater. 35 (2023) 2884–2891.
[45] Q. Fang, H. Yin, X. Mao, Y. Han, C. Yan, A.P. O'Mullane, A. Du, Theoretical evaluation of highly efficient nitrate reduction to ammonia on inbi, J. Phys. Chem. Lett. 14 (2023) 2410–2415.
[46] A. Tsoukalou, P.M. Abdala, D. Stoian, X. Huang, M.-G. Willinger, A. Fedorov, C. R. Müller, Structural evolution and dynamics of an in_2o_3 catalyst for co_2 hydrogenation to methanol: an operando xas-xrd and in situ tem study, J. Am. Chem. Soc. 141 (2019) 13497–13505.

[47] T. Bielz, H. Lorenz, W. Jochum, R. Kaindl, F. Klauser, B. Klotzer, S. Penner, Hydrogen on in_2o_3: reducibility, bonding, defect formation, and reactivity, The Journal of Physical Chemistry C 114 (2010) 9022–9029.

[48] G. Kresse, J. Hafner, Ab initio molecular dynamics for liquid metals, Phys. Rev. B 47 (1993) 558.

[49] G. Kresse, J. Furthmüller, Efficient iterative schemes for ab initio total-energy calculations using a plane-wave basis set, Phys. Rev. B 54 (1996) 11169.

[50] P.E. Blöchl, Projector augmented-wave method, Phys. Rev. B 50 (1994) 17953.

[51] J.P. Perdew, J.A. Chevary, S.H. Vosko, K.A. Jackson, M.R. Pederson, D.J. Singh, C. Fiolhais, atoms, molecules, solids, and surfaces: applications of the generalized gradient approximation for exchange and correlation, Phys. Rev. B 46 (1992) 6671.

[52] J.P. Perdew, Y. Wang, Accurate and simple analytic representation of the electron-gas correlation energy, Phys. Rev. B 45 (1992) 13244.

[53] A. Jain, S.P. Ong, G. Hautier, W. Chen, W.D. Richards, S. Dacek, S. Cholia, D. Gunter, D. Skinner, G. Ceder, Commentary: the materials project: a materials genome approach to accelerating materials innovation, APL. Mater. (2013) 1.

[54] S. Grimme, Semiempirical gga-type density functional constructed with a long-range dispersion correction, J. Comput. Chem. 27 (2006) 1787–1799.

[55] K. Mathew, R. Sundararaman, K. Letchworth-Weaver, T. Arias, R.G. Hennig, Implicit solvation model for density-functional study of nanocrystal surfaces and reaction pathways, J. Chem. Phys. (2014) 140.

[56] W. Tang, E. Sanville, G. Henkelman, A grid-based bader analysis algorithm without lattice bias, J.f Phys. Condensed Matter 21 (2009) 084204.

[57] E. Sanville, S.D. Kenny, R. Smith, G. Henkelman, Improved grid-based algorithm for bader charge allocation, J. Comput. Chem. 28 (2007) 899–908.

[58] T. Hu, C. Wang, M. Wang, C.M. Li, C. Guo, Theoretical insights into superior nitrate reduction to ammonia performance of copper catalysts, ACS. Catal. 11 (2021) 14417–14427.

[59] J.K. Nørskov, J. Rossmeisl, A. Logadottir, L. Lindqvist, J.R. Kitchin, T. Bligaard, H. Jonsson, Origin of the overpotential for oxygen reduction at a fuel-cell cathode, J. Phys. Chem. B 108 (2004) 17886–17892.

[60] V. Wang, N. Xu, J.-C. Liu, G. Tang, W.-T. Geng, Vaspkit: a user-friendly interface facilitating high-throughput computing and analysis using vasp code, Comput. Phys. Commun. 267 (2021) 108033.

[61] B. Zhang, N.N. Zhang, J.F. Chen, Y. Hou, S. Yang, J.W. Guo, X.H. Yang, J.H. Zhong, H.F. Wang, P. Hu, Turning indium oxide into a superior electrocatalyst: deterministic heteroatoms, Sci. Rep. 3 (2013) 3109.

[62] M.S. Frei, M. Capdevila-Cortada, R. García-Muelas, C. Mondelli, N. López, J. A. Stewart, D.C. Ferré, J. Pérez-Ramírez, Mechanism and microkinetics of methanol synthesis via co_2 hydrogenation on indium oxide, J. Catal. 361 (2018) 313–321.

[63] T.P. Araújo, J. Morales-Vidal, G. Giannakakis, C. Mondelli, H. Eliasson, R. Erni, J. A. Stewart, S. Mitchell, N. López, J. Pérez-Ramírez, Reaction-induced metal-metal oxide interactions in pd-in_2o_3/zro_2 catalysts drive selective and stable co_2 hydrogenation to methanol, Angewandte Chemie International Edition 62 (2023) e202306563.

[64] M. Wagner, S. Seiler, B. Meyer, L.A. Boatner, M. Schmid, U. Diebold, Reducing the in_2o_3 (111) surface results in ordered indium adatoms, Adv. Mater. Interfaces. 1 (2014) 1400289.

[65] J. Ye, C. Liu, D. Mei, Q. Ge, Active oxygen vacancy site for methanol synthesis from co_2 hydrogenation on in_2o_3 (110): a dft study, ACS. Catal. 3 (2013) 1296–1306.

[66] D. Albani, M. Capdevila-Cortada, G. Vilé, S. Mitchell, O. Martin, N. López, J. Pérez-Ramírez, Semihydrogenation of acetylene on indium oxide: proposed single-ensemble catalysis, Angewandte Chemie 129 (2017) 10895–10900.

[67] S.M. Gericke, M.M. Kauppinen, M. Wagner, M. Riva, G. Franceschi, A. Posada-Borbón, L. Rämisch, S. Pfaff, E. Rheinfrank, A.M. Imre, Effect of different in_2o_3 (111) surface terminations on co_2 adsorption, ACS Appl. Mater Interfaces 15 (2023) 45367–45377.

[68] M. Wagner, B. Meyer, M. Setvin, M. Schmid, U. Diebold, Direct assessment of the acidity of individual surface hydroxyls, Nature 592 (2021) 722–725.

[69] A. Cao, Z. Wang, H. Li, J.K. Nørskov, Relations between surface oxygen vacancies and activity of methanol formation from co_2 hydrogenation over in_2o_3 surfaces, ACS. Catal. 11 (2021) 1780–1786.

[70] J. Wu, Y.-X. Yu, A theoretical descriptor for screening efficient no reduction electrocatalysts from transition-metal atoms on n-doped bp monolayer, J. Colloid Interface Sci. 623 (2022) 432–444.

[71] J. Wu, Y.-X. Yu, Efficient electrocatalysts refined from metal-dimer-anchored pc_6 monolayers for no reduction to ammonia, Int. J. Hydrogen Energy 48 (2023) 5961–5975.

[72] Y. Wang, A. Xu, Z. Wang, L. Huang, J. Li, F. Li, J. Wicks, M. Luo, D.-H. Nam, C.-S. Tan, Enhanced nitrate-to-ammonia activity on copper–nickel alloys via tuning of intermediate adsorption, J. Am. Chem. Soc. 142 (2020) 5702–5708.

[73] J.-X. Liu, D. Richards, N. Singh, B.R. Goldsmith, Activity and selectivity trends in electrocatalytic nitrate reduction on transition metals, ACS. Catal. 9 (2019) 7052–7064.

[74] I. Katsounaros, M.C. Figueiredo, X. Chen, F. Calle-Vallejo, M.T. Koper, Interconversions of nitrogen-containing species on pt (100) and pt (111) electrodes in acidic solutions containing nitrate, Electrochim. Acta 271 (2018) 77–83.

[75] I. Katsounaros, M.C. Figueiredo, X. Chen, F. Calle-Vallejo, M.T. Koper, Structure- and coverage-sensitive mechanism of no reduction on platinum electrodes, ACS. Catal. 7 (2017) 4660–4667.

[76] Y. Wang, X. Qin, M. Shao, First-principles mechanistic study on nitrate reduction reactions on copper surfaces: effects of crystal facets and ph, J. Catal. 400 (2021) 62–70.

[77] D.Y. Shin, D.-H. Lim, Dft investigation into efficient transition metal single-atom catalysts supported on n-doped graphene for nitrate reduction reactions, Chem. Eng. J. 468 (2023) 143466.

[78] H. Niu, Z. Zhang, X. Wang, X. Wan, C. Shao, Y. Guo, Theoretical insights into the mechanism of selective nitrate-to-ammonia electroreduction on single-atom catalysts, Adv. Funct. Mater. 31 (2021) 2008533.

[79] H. Xu, Y. Ma, J. Chen, W.-x. Zhang, J. Yang, Electrocatalytic reduction of nitrate–a step towards a sustainable nitrogen cycle, Chem. Soc. Rev. 51 (2022) 2710–2758.